Ruby at high pressure. I. Optical line shifts to 156 GPa

Jon H. Eggert, Kenneth A. Goettel, and Isaac F. Silvera
Lyman Laboratory of Physics, Harvard University, Cambridge, Massachusetts 02138
(Received 13 March 1989)

We have measured the pressure shifts of the ruby R lines and several surrounding lines to 156 GPa in a quasihydrostatic xenon pressure medium. We fit these lines to a cubic crystal-field scaling theory, including trigonal field distortions and spin-orbit coupling as perturbations. By scaling with volume, rather than pressure, we obtained good agreement with the observed curvature in the line shifts with pressure. Measurements of the R_3' line to 140 GPa in a nonhydrostatic environment yielded R_3' line shifts similar to those observed in the quasihydrostatic measurements. We also measured the U absorption band shift to 106 GPa in a nonhydrostatic environment and found good agreement with our scaling theory. We infer a U-band–B-line anticrossing near 70 GPa and predict an R_3'-R line crossing near 200 GPa. The implications of these results to pressure measurements using the ruby pressure scales are discussed.

I. INTRODUCTION

The pressure dependence of the ruby R_1 line (see Fig. 1) is widely used to determine pressures in diamond-anvil-cell experiments.[1,2] The ruby R_1 pressure scale has been calibrated to 80 GPa under quasihydrostatic conditions[3] and to 180 GPa under nonhydrostatic conditions.[4] Recently, however, experimental results have been reported in the 150–250-GPa range[5,6] using extrapolations of the quasihydrostatic ruby pressure scale and in the 450–550-GPa range[7,8] using extrapolations of the nonhydrostatic ruby pressure scale. These extrapolations to approximately 3 times the calibrated pressure range underscore the need for a better understanding of the spectra of ruby at ultrahigh pressures.

High-pressure electronic transitions in ruby, other than the R_1 line, have not been studied extensively. Several investigators have studied the pressure dependence of the electronic transitions in ruby to 15 GPa (Refs. 9–12) and shock measurements of the broad absorption bands have been made to over 50 GPa.[13,14] We have measured the spectra of a number of lines near the R lines to 156 GPa, and have measured the U-band pressure shift to 106 GPa. Fits of these data to a crystal-field scaling theory give insight into the high-pressure electronic structure of ruby and into the use of the ruby pressure scale at very high pressures.

We begin with a review of the electronic structure of ruby in the following section. In Secs. III and IV the experimental measurements are presented and discussed. Sections V and VI are devoted to a discussion of ruby as a pressure measurement standard and conclusions. In a companion article, results of ruby R-line lifetime measurements to 130 GPa are presented.

II. REVIEW OF THE RUBY CRYSTAL AND ELECTRONIC STRUCTURE

The crystal structure of ruby consists of a corundum (Al_2O_3) lattice with impurity chromium ions (Cr^{3+}) substituted for aluminum ions.[15,16] Corundum is a hexagonal-close-packed oxygen lattice with aluminum occupying two-thirds of the octahedral sites. The site symmetry of these octahedral sites would be cubic O_h if no distortions occurred. However, repulsive interactions between neighboring aluminum ions introduce a slight trigonal distortion, reducing the aluminum site symmetry to

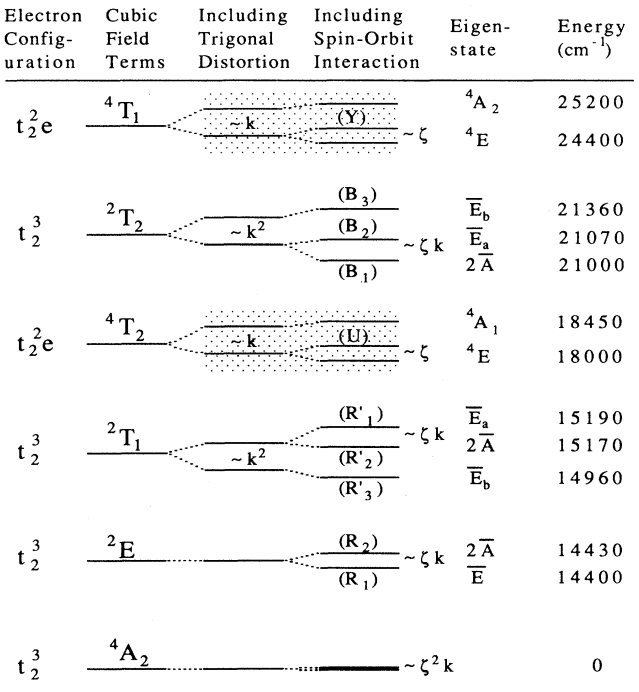

FIG. 1. A summary of the ambient-pressure electronic structure of ruby for transitions in the visible energy region. The transition energies are from the compilation by Mcfarlane (Ref. 30). The notation for transitions to the ground state is shown in parentheses. The dependence of the splittings upon the trigonal field distortion ($k \sim \langle t_2 | V_{tr} | t_2 \rangle$) and the spin-orbit interaction ($\xi \sim \langle t_2 | \mathcal{H}_{so} | t_2 \rangle$) are shown.

C_3. This trigonal distortion removes the inversion symmetry of the aluminum sites.

Ligand-field theory has been successful in describing the electronic excitations of ruby.[17] The electronic states for the three chromium valence d electrons are first treated in the strong-field scheme for the Coulomb interaction in the cubic approximation (site symmetry O_h). The trigonal distortion and spin-orbit interaction are treated as perturbations.

The effect of a cubic field on d electrons is to split the single-electron wave function into two states designated by their symmetry labels, t_{2g} and e_g. All states in the cubic-field approximation are of even parity and we subsequently drop the subscript g. The energy of the e state is higher than that of the t_2 state by a factor of 10 times the cubic crystal-field parameter Dq.[17] The distribution of the d electrons into these states is called the electron configuration. In O_h symmetry, t_2^3 is the lowest-energy electron configuration (see Fig. 1).

For d^3 electrons, O_h symmetry leads to the energy terms $^4A_2(t_2^3)$, $^2E(t_2^3)$, $^2T_1(t_2^3)$, $^4T_2(t_2^2e)$, $^2T_2(t_2^3)$, and $^4T_1(t_2^2e)$ in the visible energy region. Transitions between the upper states and the ground state ($^4A_2$) are denoted R, R', U, B, and Y, respectively. We use the term notation when referring to a specific energy state and the transition notation when referring to transitions to the ground state. In Fig. 1 we give the notation for transitions to the ground state in parentheses. Given the cubic-field parameter Dq and the two Racah parameters B and C, the term energies may be calculated by diagonalizing the energy matrices given by Sugano *et al.*[17] The transition energies between terms with different electron configurations (U, Y) depend strongly upon the crystal-field parameter Dq and result in broad bands, while transitions between terms with the same configuration (R, R', B) depend weakly upon Dq and result in narrow lines.[17]

The trigonal distortion (V_{tr}) and spin-orbit coupling ($\mathcal{H}_{so}$) can connect different terms ($\langle\Gamma|V_{tr}|\Gamma'\rangle$, $\langle\Gamma|\mathcal{H}_{so}|\Gamma'\rangle\neq 0$, where Γ and Γ' are O_h-symmetry terms). The coupling scheme for V_{tr} and $\mathcal{H}_{so}$ among different terms[18] is shown in Fig. 2. Such couplings give rise to energy-level splittings. Figure 1 shows the dependence of the splittings upon the trigonal and spin-orbit perturbations (here $k\sim\langle t_2|V_{tr}|t_2\rangle$, $\zeta\sim\langle t_2|\mathcal{H}_{so}|t_2\rangle$).[18] The $^4T_1$ and the $^4T_2$ levels are split by the trigonal field alone, while the $^2T_1$ and the $^2T_2$ levels are split in second order. The $^4A_2$ and the ^2E levels are split by the combined effect of the trigonal field and the spin-orbit interaction.

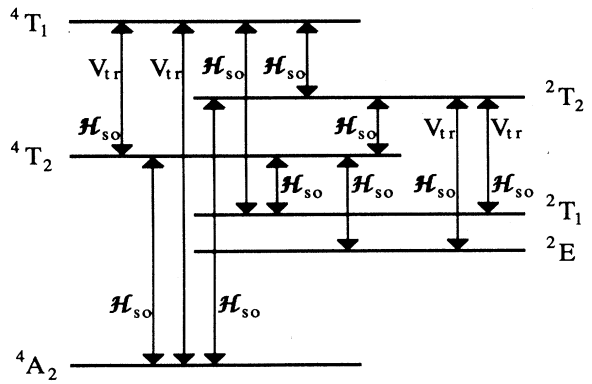

FIG. 2. The couplings between cubic-field terms due to the trigonal field distortion (V_{tr}) and the spin-orbit interaction ($\mathcal{H}_{so}$) (after Sugano *et al.*) (Ref. 18).

Surrounding the intense R lines are many weak satellite lines caused by static and dynamic distortions of the crystal field. The presence of neighboring Cr^{3+} impurities perturbs the local crystal field and gives rise to neighbor lines. The most prominent of these neighbor lines, arising from third- and fourth-nearest neighbors, are denoted N_1 and N_2, respectively, and lie on the low-energy side of the R_1 line.[19] Interactions with lattice phonons give rise to vibronic sidebands shifted from the R lines by the absorption or emission of phonons.

III. EXPERIMENTAL METHODS

We report results on ruby (0.5 wt.% Cr^{3+}) in two different experimental conditions. First, we studied ~2-μm-diam ruby grains in a quasihydrostatic xenon pressure-transmitting medium.[5] We measured ruby line positions and intensities in the frequency range 12 500–15 500 cm^{-1} at pressures up to 156 GPa. Pressures were determined by the quasihydrostatic ruby calibration.[3] Second, we determined the absorption U-band shift to 106 GPa and the R_3' line shift to 140 GPa on ~1–5-μm-diam ruby grains at a diamond-rhenium gasket interface. In this nonhydrostatic environment we used the nonhydrostatic pressure calibration.[4]

The pressure cell was a slightly modified Mao-Bell–type diamond-anvil cell.[20] We used double-beveled diamond anvils and rhenium gaskets in all of the experiments.[7,21,22] A liquid-nitrogen-cooled box and a scheme similar to that described by Silvera and Wijngaarden[23] was used to load the xenon pressure-transmitting medium[5] in the quasihydrostatic measurements.

Our optical system consisted of a microscope system with several optical ports, allowing the entrance of a laser beam, visual viewing of the sample, and signal output.[24] This system focused argon-ion laser light to a spot size less than 5 μm in diameter. Unless stated otherwise, we used the argon-ion laser line at 458 nm for all measurements. A sample stage with three-axis translation allowed 1-μm positioning resolution of the sample. Spatial filtering of the ruby fluorescence signal, with a pinhole located at a real image of the sample, allowed us to limit the sampling-area diameter to 4 μm. We coupled the fluorescence signal into a high-throughput grating spectrometer, where the light was detected with an intensified diode array.

Identification of the ruby lines was achieved at ambient pressure using a 1200-groove/mm grating [full width at half maximum (FWHM) resolution ~10 cm^{-1}]. High-pressure spectra (Fig. 3) were taken using a 300-groove/mm grating (FWHM resolution ~40 cm^{-1}), in addition to the 1200-groove/mm grating. In the quasihy-

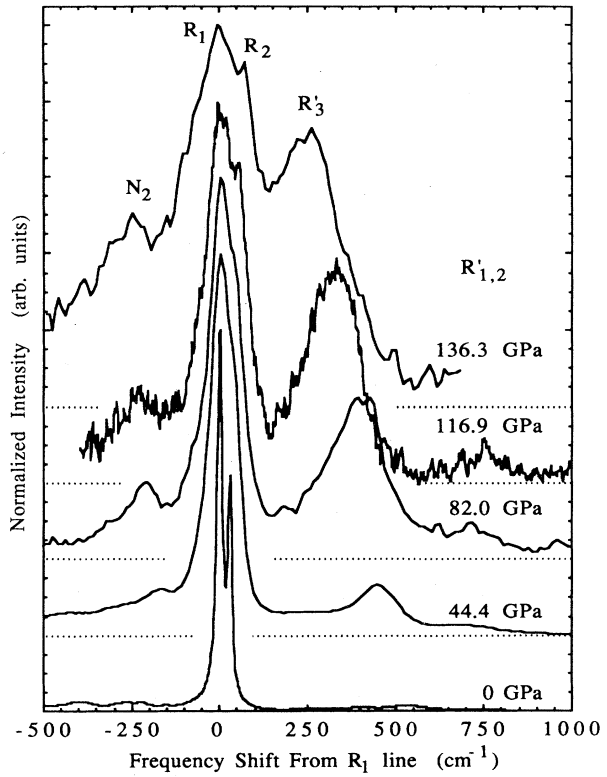

FIG. 3. Ruby fluorescence spectra at various pressures in the quasihydrostatic pressure medium. To facilitate comparison of spectra at different pressures, we plot the frequency relative to the R_1-line frequency at each pressure. The R_1 line shifts with pressure as shown in Fig. 4. The spectra are normalized to their maximum intensities and vertically offset for clarity.

drostatic xenon sample, we followed the two R lines, the R_3' line, an unresolved doublet of the R_1' and R_2' lines (R_{12}'), and one neighbor line (N_2) to 156 GPa. We followed another neighbor line (N_1) and a vibronic sideband on the low-energy side of the R_1 line to 82.5 GPa. Due to more rapid broadening of the N_1 line, we were unable to follow the N_1 line to as high a pressure as the N_2 line. This is consistent with other observations that have found greater microscopic strain broadening in the N_1 line.[25]

The width of the lines was such that significant overlap existed among adjacent lines and the intense R lines (see Fig. 3). To measure line-center frequencies and integrated intensities, we fit a convolution of Lorentzians to the measured spectrum at each pressure. The pressure dependence of the observed lines is shown in Fig. 4. All of the lines display red shifts similar to that of the R_1 line. We note that the R_1 line broadens more rapidly than does the R_2 line, and that the R_1-R_2 line separation at the highest pressure was $\sim 100\ \mathrm{cm}^{-1}$.

We determined the pressure shift of the $^4T_2$ state (U band) up to 106 GPa by measuring the R-line luminescence intensity as a function of U-band excitation wavelength for three argon-ion laser lines (514, 488, and 458

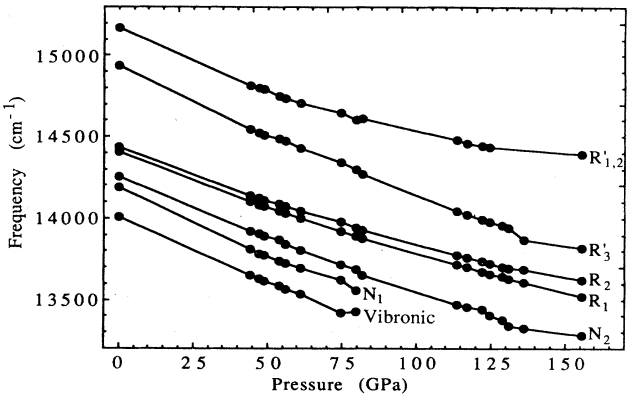

FIG. 4. The pressure shifts of the peak frequency for the seven lines which we studied. The drawn lines simply connect the data points as a visual aid.

nm) in the nonhydrostatic sample. This is possible, when the transition is not power saturated, because the ^2E level is populated by very rapid nonradiative transitions from the $^4T_2$ level.[26] More importantly, the quantum efficiency, defined as the ratio of the number of fluorescent R-line photons to the number of absorbed photons, is nearly constant over the U and Y absorption bands.[27] Thus, at a given pressure for excitation at a given frequency, the R-line luminescence intensity is proportional to the U-band absorption efficiency.

IV. RESULTS AND DISCUSSION

A. Fits in the cubic (O_h) Coulomb approximation

We fit the R and R' lines to a scaling theory developed by Munro[28] which was able to predict the red and blue line shifts of the electronic transitions in ruby up to 10 GPa. He assumed hydrostatic pressure and no structural phase transitions. These two assumptions are supported by x-ray diffraction measurements on ruby in which the c/a ratio was fairly constant and no phase transitions were detected up to 175 GPa.[29] Munro scaled the electronic charge (e) and nuclear charge number (z) with pressure:

$$e^2 \rightarrow \varepsilon^2 \equiv \Lambda(P)e^2, \quad z \rightarrow Z \equiv \frac{\Omega(P)}{\Lambda(P)} z \ .$$

$\Lambda(P)$ and $\Omega(P)$ are scaling parameters with $\Lambda(0) = \Omega(0) = 1$. By scaling the cubic crystal field and Racah parameters (Dq, B, C) in this way, Munro derived a simple expression for the shift of any line in terms of $\Omega(P)$ and $\Lambda(P)$:

$$\frac{\delta E}{E_0} = \beta \frac{\delta D}{D} + (2-\beta)[\Lambda(P)-1] + (1-5\beta)[\Omega(P)-1] \ ,$$

where

$$\beta \equiv \left[\frac{x_0}{y_0}\right]\left[\frac{dy}{dx}\right]_0, \quad x \equiv \frac{Dq}{B}, \quad y \equiv \frac{E}{B} \ .$$

In this expression $\delta D/D$ is determined by the equation of state,[28] and β is found from the energy matrices given by Sugano *et al.*[17] Munro was able to limit the number of adjustable parameters to two by assuming a linear dependence of the scaling parameters upon pressure:

$$\Omega(P)=1+\delta\Omega P, \quad \Lambda(P)=1+\delta\Lambda P \ .$$

Using $\delta\Omega=1.5\times10^{-4}$ GPa^{-1} and $\delta\Lambda=-4.5\times10^{-4}$ GPa^{-1}, he achieved good results up to 10 GPa, below which all line shifts are linear with pressure. In reproducing Munro's work, using $B=650$ cm^{-1} and $C=3120$ cm^{-1}, we found $\beta(R)=0.0340$, $\beta(R')=0.0236$, $\beta(U)=1.000$, $\beta(B)=0.131$, and $\beta(Y)=0.788$. For E_0 we used cubic-field line centers, determined from the data given by Mcfarlane[30] averaged over the appropriate splittings.

We believe that a somewhat more realistic but still simple behavior for Ω and Λ is to scale linearly with the volume difference:

$$\Omega(P)=1+\delta\Omega dV, \quad \Lambda(P)=1+\delta\Lambda dV \ ,$$

where

$$dV\equiv\frac{V(P)-V_0}{V(P)} \ ,$$

V is the molar volume, and V_0, the ambient-pressure volume, is 25.6 cm^3/mol.[31] We averaged our data for the split components of the R and R' lines to give a cubic-field line center $[E_R=\frac{1}{2}(E_{R_1}+E_{R_2}),\ E_{R'}=\frac{1}{3}(2E_{R'_{12}}+E_{R'_3})]$. Using these pressure-shift data, we found best-fit values for $\delta\Omega$ and $\delta\Lambda$ to be $\delta\Omega=-0.051(7)$ and $\delta\Lambda=0.129(3)$. We used a Birch-Murnaghan equation of state:

$$P(f)=3K_0f(1+2f)^{5/2}(1+a_1f) \ ,$$

where

$$f=\frac{1}{2}\left[\left(\frac{V_0}{V}\right)^{2/3}-1\right], \quad a_1=\tfrac{3}{2}(K'_0-4) \ ,$$

with $K_0=254$ GPa and $K'_0=4.3$.[29,31] In Fig. 5(a) we show that below ~30 GPa our fit, scaling with dV, reproduces Munro's fit, scaling with pressure. At higher pressures, our fit closely follows the observed nonlinearity in both the R and R' line-center shifts versus pressure. A slight difference exists between the quasihydrostatic pressure calibration and our fit to the R line at pressures above 100 GPa. This disagreement is fairly minor, considering the simplicity of the assumptions in our fit and the fact that the quasihydrostatic scale has been calibrated only to 80 GPa. The pressure shifts predicted for all transitions by our fit are shown by the solid lines in Fig. 5(b). Considering the scatter in the available data, our fit is in good agreement with previous measurements of the R', B, U, and Y transition pressure shifts.

Ma *et al.*[32] have also developed a scaling theory similar to Munro's. However, it requires seven adjustable parameters and predicts a turnover in the crystal-field parameter, Dq, at around 50 GPa. The Dq behavior is reflected by the turnover in the fit by Ma *et al.* to the U- and Y-band energies shown by the dashed lines in Fig. 5(b). The monotonically increasing behavior of Dq in our scaling method (using two adjustable parameters) fits our new high-pressure data better than does the theory by Ma *et al.* Ohnishi and Sugano[33] have developed a quantum-mechanical theory for the pressure response of the energy states of an octahedral $[CrO_6]^{9-}$ cluster. Their results for the pressure shift of the U band and the R line are in agreement with our fits at low pressure but tend to diverge at pressures above about 10 GPa.

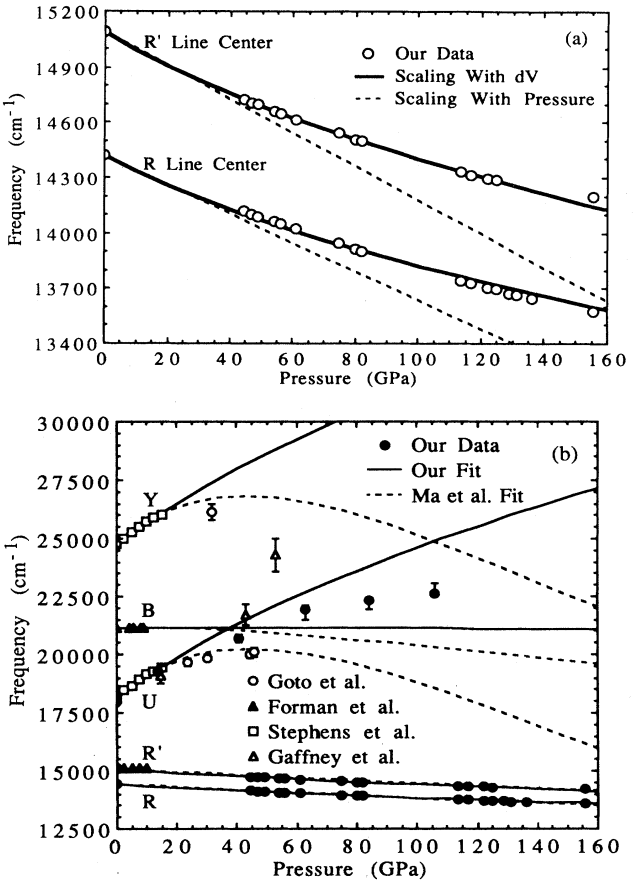

FIG. 5. (a) The pressure dependence of the R- and R'-line centers, and two variations of Munro's scaling theory (Ref. 28). The solid lines scale Λ and Ω linearly with dV (present work), while the dashed lines scale linearly with pressure (Munro). (b) Our data, including our U-band shift data, along with previous absorption measurements (Refs. 9, 10, 13, and 14). Our fit, scaling Λ and Ω with dV, is shown by solid lines. The dashed lines indicate the results for the scaling theory developed by Ma *et al.* (Ref. 32).

B. *U*-band absorption fits

Our technique for determining the U-band absorption shift, by measuring the R-line fluorescence intensity versus pump frequency, requires a model U-band absorption line shape. Our three U-band absorption data (pumped at 514, 488, and 458 nm) were fitted to the quantum-mechanical single-configuration-coordinate (QMSCC) model given by Struck and Fonger[34] for phonon-assisted radiative excitation to a Franck-Condon (FC) offset level. For a review of the single-

configuration-coordinate (SCC) model, see the article by Klick and Schulman.[35] The QMSCC model uses parameters from the SCC diagram: The Manneback angle θ, which is related to the relative parabola force constants (phonon energies) of the upper (v) and lower (u) states, the offset parameter a_{uv}, which is a measure of the FC offset, the phonon energies $\hbar\omega_{u,v}$, and the zero-phonon energy difference $h\nu_0$. Fonger and Struck[36] gave the relevant parameters for U-band σ- ($E\perp c$) polarization absorption at room temperature as $\theta=44°$, $a_{uv}=3.526$, $\hbar\omega_v=500$ cm^{-1}, and $h\nu_0=16\,480$ cm^{-1}. For π ($E\|c$) polarization they suggested identical parameters except that $h\nu_0=17\,010$ cm^{-1}. The measured oscillator strength for σ polarization is about 2 times that for π polarization.[26] For our unoriented ruby we assumed a weighted average line shape,

$$I(\omega)=\tfrac{1}{5}\{2[2I_\sigma(\omega)]+I_\pi(\omega)\} .$$

The additional factor of 2 is due to the two equivalent σ polarizations. We assumed that θ and a_{uv} are constant as a function of pressure, and that $\hbar\omega_v$ has the volume (pressure) dependence appropriate for a constant overall Grüneisen parameter of $\gamma=1.3$.[37] We varied $h\nu_0$ and a multiplicative scaling factor for the best fit to our data (Fig. 6). The experimental points represent a chi-squared fit to all three data points, and the error bars represent the spread in the zero-phonon energy obtained by equally weighted pairs of data. The first moment of the band, defined as

$$h\nu_1=h\nu_0+\hbar\omega_v S_v, \quad S_v=\tfrac{1}{2}(a_{uv}\sin\theta)^2$$

approximates the band peak. We plot both the zero-phonon energy and the first moment of the band in Fig. 6.

When our U-band data is plotted with our scaling-theory fits [Figs. 5(b) and 6], we note that although the first moment of the U band crosses the B line with no effect, the zero-phonon energy ($h\nu_0$) approaches the B line asymptotically. This is the behavior expected near a line crossing for interacting states. From Fig. 2, we see that the $^4T_2$ state and the $^2T_2$ states are coupled by the spin-orbit interaction ($\mathcal{H}_{so}$). $\mathcal{H}_{so}$ is given by the sum of one-electron operators $\xi(r)(\mathbf{l}\cdot\mathbf{s})$, where

$$\xi(r)=-\frac{e\hbar^2}{2m^2c^2}\frac{1}{r}\frac{dV(r)}{dr} ,$$

and V is the potential in which the electron moves.[17]

We make the simplifying assumption that $\mathcal{H}_{so}(P)\sim Dq(P)$. This assumption, while not rigorously justified, gives adequate fits to both our U-band–B-line crossing data and our R_1-R_2 line-splitting data. From our scaling-theory fits we find $Dq\sim 1-1.462dV$. Letting $M=\langle {}^2T_2|\mathcal{H}_{so}|{}^4T_2\rangle$ be the energy-matrix mixing element and diagonalizing the resulting energy matrix, we find two mixed states,

$$|+\rangle=u_+|{}^4T_2\rangle+b_+|{}^2T_2\rangle ,$$
$$|-\rangle=u_-|{}^4T_2\rangle+b_-|{}^2T_2\rangle ,$$

where

$$(u_\pm)^2=\frac{4M^2}{4M^2+(E_B-E_U\pm\eta)^2} ,$$
$$(b_\pm)^2=\frac{(E_B-E_U\pm\eta)^2}{4M^2+(E_B-E_U\pm\eta)^2} ,$$
$$\eta^2=(E_B-E_U)^2+4M^2 .$$

E_B and E_U are the zero-phonon energies of the unperturbed B and U transitions, respectively, and the energy eigenvalues are

$$\lambda_\pm=\tfrac{1}{2}(E_B+E_U\pm\eta) .$$

Note that for low pressures $|+\rangle\rightarrow|{}^2T_2\rangle$, $|-\rangle\rightarrow|{}^4T_2\rangle$, and for high pressures $|+\rangle\rightarrow|{}^4T_2\rangle$, $|-\rangle\rightarrow|{}^2T_2\rangle$. Our U-band absorption data are well described by this anticrossing model, using the energy shifts of the $^4T_2$ and the $^2T_2$ levels predicted by our scaling theory and the ambient-pressure value of $M_0=700$ cm^{-1} (Fig. 6). The matrix elements of the spin-orbit interaction have been calculated,[17] and yield $\langle {}^2T_2|\mathcal{H}_{so}|{}^4T_2\rangle=\sqrt{6}\zeta'$. Using $\zeta'=170$ cm^{-1} implies that $M_0=416$ cm^{-1}; our ambient-pressure value of M is seen to be larger than, but of the same magnitude as, the predicted value.[38]

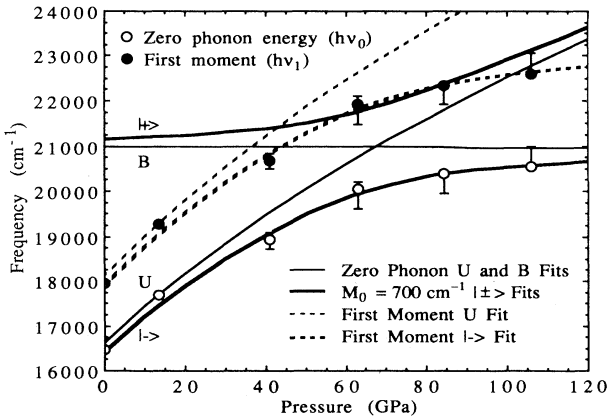

FIG. 6. Our U-band absorption data. The open circles and solid lines indicate the zero-phonon energy of the $^4T_2$ band in σ polarization. The thin lines are from our scaling-theory fit, while the thick lines are fitted to an anticrossing theory with $M_0=\langle {}^4T_2|\mathcal{H}_{so}|{}^2T_2\rangle=700$ cm^{-1}.

C. The R- and R'-line splittings

Although our adaptation of Munro's theory gives good fits to the R- and R'-line centers, we would also like to fit the individual split components. The splitting of the R'_{12} and R'_3 lines ($\Delta R'$) is proportional to the square of the trigonal field parameter (k^2) (Fig. 1), and we found a good fit to the data shown in Fig. 7(a) for

$$\Delta R'=228+5100(-dV)^{2.65} .$$

We note that k is dependent upon the degree of nonhydrostatic stresses in the ruby sample[39–41] and that this is not a universal relation for k. Similarly, the splitting of

the R_1 and R_2 lines (ΔR) is proportional to the product of the trigonal field parameter and the spin-orbit-coupling parameter ($k\zeta$). Using the assumption made earlier that the spin-orbit coupling is proportional to Dq, and the value of k found for the R'-line splitting, we find the fit shown in Fig. 7(b),

$$\Delta R = 2.07[228 + 5100(-dV)^{2.65}]^{1/2}(1 - 1.462dV) .$$

Combining our line-center fits [Fig. 5(a)] with these line-splitting fits, we achieved the fits to the R- and R'-line components shown in Fig. 7(c).

Our data suggest that the R_3' line will cross the R lines near 200 GPa. We note that unlike the $^4T_2$-$^2T_2$ level crossing discussed earlier, neither the trigonal nor the spin-orbit perturbations couple the ^2E and the $^2T_1$ levels.[17,18] Therefore, the R_3' and the R lines should cross one another unperturbed.

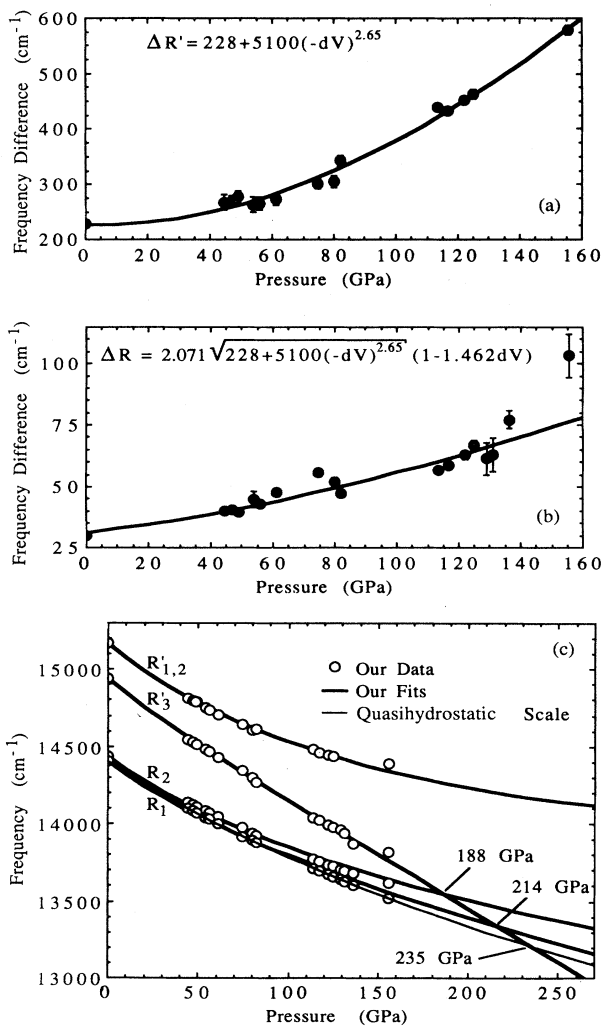

FIG. 7. (a) The R' splitting fit to the empirical function $\Delta R' \sim k^2 = A[1 + B(-dV)^C]$. (b) The R splitting fitted to $\Delta R \sim k\zeta$, assuming that k varies with pressure as in (a), and ζ varies as the crystal-field parameter $Dq \sim 1 - 1.462dV$. (c) The fits obtained by combining our cubic-field scaling fit with our fits to the line splittings. Note that the R_3' line is predicted to cross the R lines at pressures near 200 GPa. The quasihydrostatic pressure scale of Mao *et al.* (Ref. 3) is also shown.

D. Line intensities

The integrated intensities of the R' lines relative to the R lines increase dramatically with pressure (Fig. 3). The R_3' shows the greatest increase in relative intensity, rising from 7% at ambient pressure to approximately 100% above 130 GPa (Fig. 8). This increase in relative intensity must be accounted for by relative changes in the populations and or transition rates of the states. The ^2E and $^2T_1$ levels, as well as those responsible for the N lines are in thermal equilibrium at 300 K.[26,42] The relative populations in these levels obey a Boltzmann distribution and depend upon pressure as their relative energies shift. Although the population in the $^2T_1$ state relative to the ^2E state increases with pressure, this increase is not sufficient to explain our data. It appears that a relative change in the transition rates must be invoked to explain our observations.

E. Nonhydrostatic measurements of R_3'

In Fig. 9(a) we show a nonhydrostatic ruby spectrum at 109 GPa, obtained on a rhenium gasket, together with a quasihydrostatic ruby spectrum at 114 GPa, obtained from a ruby in xenon. The observed increasing intensity of the R_3' line and our fit to its pressure shift allow us to identify the shoulder on the high-energy side of the R lines in the nonhydrostatic spectrum as the R_3' line. We measured the position of the R_3' shoulder in a number of nonhydrostatic rubies [Fig. 9(b)]. None of the rubies we measured above 140 GPa displayed this R_3' shoulder, due to the diminishing line separation and the broad width of the lines.

The nonhydrostatic R_3' line is shifted to a lower frequency from its quasihydrostatic position. This is the expected behavior since the R'-line splitting should be larger due to the increased trigonal distortion in a nonhydrostatic environment. The similarity of the pressure dependence of the nonhydrostatic splittings to the quasihydrostatic splittings is striking. Two explanations

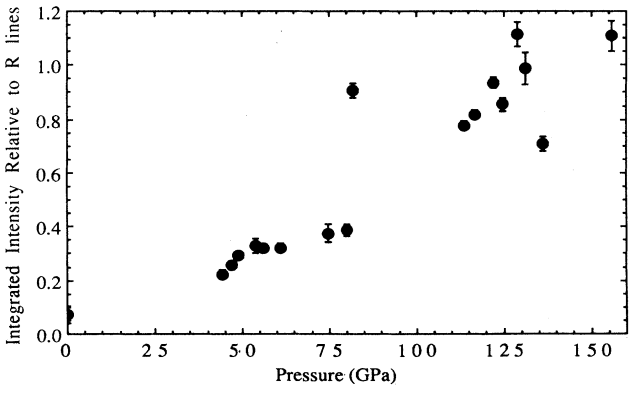

FIG. 8. The R_3' integrated intensity relative to the R lines showing the strong increase in intensity with pressure.

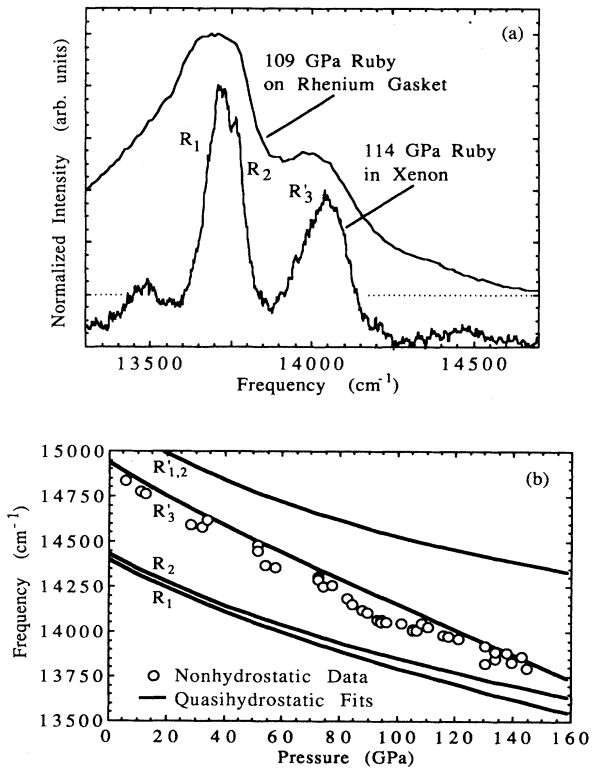

FIG. 9. (a) Spectra taken in nonhydrostatic (rhenium gasket) and quasihydrostatic (xenon sample) environments at similar pressures determined by the appropriate ruby calibration. We identify the shoulder in the nonhydrostatic spectrum, on the high-frequency side of the R lines as the R_3' line. (b) Our measurements of the R_3' shoulder in nonhydrostatic measurements plotted along with our quasihydrostatic line fits.

may be postulated; one, the quasihydrostatic ruby is not very hydrostatic, and two, the increasing trigonal distortion at high pressure is not due entirely to nonhydrostatic stresses. It is reasonable to assume that each of these postulates is true to a degree. We note that in assessing the nonhydrostatic stress of a given sample, the R'-line splitting, which is independent of the spin-orbit coupling, may be a better gauge than the R-line splitting which has been commonly used.[41,43]

V. IMPLICATIONS FOR RUBY PRESSURE MEASUREMENTS

A. Gradients in nonhydrostatic pressure measurements

Nonhydrostatic measurements of the ruby lines generally yield broadened lines, due largely to pressure gradients.[44] We have observed substantial nonhydrostatic line narrowing in areas of sparse ruby coverage when compared to areas of heavy ruby coverage. We have observed a similar effect when the sampling area is decreased by spatial filtering. Lorenzana *et al.*[45] have shown that the effect of spatial averaging is to underestimate the peak pressure. These observations indicate that in the presence of pressure gradients small sampling areas are advisable.

B. Nonhydrostatic and quasihydrostatic calibration scales

At high pressures the nonhydrostatic[4] and quasihydrostatic[3] pressure scales show a large difference in pressure for a given R_1-line frequency (Fig. 10). If nonhydrostatic measurements measure an average peak due to broad, unresolved R_1-R_2 peaks, then for a given frequency shift the nonhydrostatic scale should give a higher pressure than the hydrostatic scale. Likewise, if frequency pulling by either decreasing fluorescence efficiency at higher pressures or spatial averaging over pressure gradients[45] were responsible for the difference, then the nonhydrostatic scale should yield a higher pressure for a given line shift. The actual calibrations, however, exhibit the opposite behavior, with the nonhydrostatic scale yielding lower pressures than the hydrostatic scale (Fig. 10).

In the nonhydrostatic calibration to 100 GPa by Mao *et al.*,[6] a discussion was given of the possible underestimation of pressure (average stress) due to differing normal and horizontal stresses in the x-ray measurements. This effect has also been discussed by Wilburn and Basset,[47] who found a large effect for relatively stiff materials. If this is the true cause of the difference in the nonhydrostatic and quasihydrostatic pressure scales, and if the nonhydrostatic pressure scale underestimates the true pressure (as originally proposed by Mao *et al.*[3,46]), then perhaps the quasihydrostatic scale is the better calibration to use in all cases. At high pressures, where the

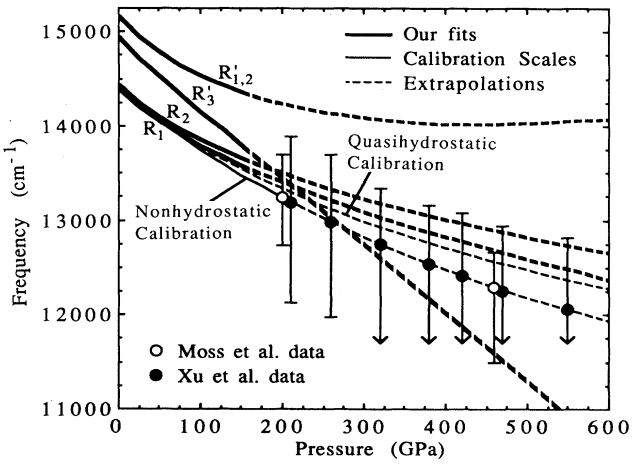

FIG. 10. The ultrahigh-pressure ruby fluorescence peaks reported by Moss *et al.* (Ref. 7) and Xu *et al.* (Ref. 8) are shown along with their widths at half maximum indicated by the vertical bars. The low-frequency widths of Xu's data at the highest pressures are undetermined due to a truncation of the experimental data. Our line fits along with the nonhydrostatic and quasihydrostatic calibrations are shown with the regions of extrapolation dashed. We note that the widths of the ultrahigh-pressure ruby spectra span the extrapolations of the R_1, R_2, and R_3' lines.

two scales differ greatly, pressures in nonhydrostatic experiments may have been systematically underestimated. More theoretical and experimental work on the effects of nonhydrostatic stress on ruby at high pressures is needed.

C. Pressure estimates at ultrahigh pressures

Moss *et al.*[7] and Xu *et al.*[8] have observed ruby fluorescence that when assigned to the R_1 line yielded pressures in the 450–550-GPa region by extrapolation of the nonhydrostatic ruby calibration.[4] The accuracy of these extreme pressures is uncertain because of the long extrapolation from the ruby calibration which extends only to 180 GPa (in Fig. 10 extrapolations are shown by dashed lines). Our observation of the rapidly increasing strength of the R_3' line and the proposed R_3'-R line crossing raises questions about the identity of the line(s) responsible for the observed fluorescence. In Fig. 10, we plot the observed ultrahigh-pressure ruby peaks[7,8] and their widths at half maximum. The lines are very broad, encompassing the line positions expected for the R_1, R_2, and R_3' lines from extrapolation of our data. If the R_3' line gives a significant contribution to the fluorescence intensity after the line crossing, then assignment of the broad ultrahigh-pressure ruby fluorescence peaks to the R_1 line may result in an overestimation of the pressure. Questions have been raised as to whether these ultrahigh-pressure fluorescence peaks are due to ruby or diamond.[48] However, recent results suggest that these fluorescence peaks are due to ruby.[49] In future experiments chopping of the fluorescence signal should aid this identification.[24]

VI. CONCLUSION

The ruby pressure scale has potential to continue to be a simple, accurate pressure-determination technique up to the highest pressures currently obtainable. However, caution regarding its assumed degree of accuracy and its use at ultrahigh pressures is advisable. As discussed above, use of the nonhydrostatic pressure scale may result in substantial systematic underestimation of ultrahigh pressures, while misidentification of the R_1 and R_3' lines may result in substantial overestimation of ultrahigh pressures. Reduction of the uncertainty about the accuracy of ultrahigh-pressure measurements requires calibration of ruby fluorescence to higher pressures, better understanding of the effects of nonhydrostatic stress on the spectra of ruby, and reconsideration of the effects of nonhydrostatic stress upon pressure determinations using x-ray diffraction and equations of state. In nonhydrostatic environments, the optical sampling area should be minimized to reduce the effects of pressure gradients. In light of these various effects it may be important to consider the experimental parameters of the calibration and the experiment in order to determine accurately the pressure of an experiment.

Several questions about the electronic behavior of ruby at high pressure remain unresolved. We do not have a complete explanation for the large increase in intensity of the R' lines relative to the R lines. The effects of nonhydrostatic stress on the spectra of ruby need to be explored more fully, both theoretically and experimentally. The need for calibrations to higher pressures and for understanding of the unresolved questions about ruby indicate that high-pressure investigation of ruby should continue to be an important research area.

ACKNOWLEDGMENTS

We thank H. Lorenzana for useful discussions and J. Brisson for help with the fitting routine computer programs. We thank R. Hemley, R. Jeanloz, and A. Ruoff for comments regarding the manuscript. This work received support from Harvard Materials Research Laboratory–National Science Foundation Grant No. DMR-14003 and National Aeronautics and Space Administration Grant No. NAGW-657.

[1]G. J. Piermarini, S. Block, J. D. Barnett, and R. A. Forman, J. Appl. Phys. **46**, 2774 (1975).
[2]A. Jayaraman, Rev. Sci. Instrum. **57**, 1013 (1986).
[3]H. K. Mao, J. Xu, and P. M. Bell, J. Geophys. Res. **91**, 4673 (1986).
[4]P. M. Bell, J. A. Xu, and H. K. Mao, in *Shock Waves in Condensed Matter,* edited by Y. M. Gupta (Plenum, New York, 1986), p. 125.
[5]K. A. Goettel, J. H. Eggert, I. F. Silvera, and W. C. Moss, Phys. Rev. Lett. **62**, 665 (1989).
[6]R. J. Hemley and H. K. Mao, Phys. Rev. Lett. **61**, 857 (1988).
[7]W. C. Moss, J. O. Hallquist, R. Reichlin, K. A. Goettel, and S. Martin, Appl. Phys. Lett. **48**, 1258 (1986).
[8]J. A. Xu, H. K. Mao, and P. M. Bell, Science **232**, 1404 (1986).
[9]D. R. Stephens and H. G. Drickamer, J. Chem. Phys. **35**, 427 (1961).
[10]R. A. Forman, B. A. Weinstein, and G. Piermarini, in Spectroscopie des Elements de Transition et des Elements Lourds dans les Solides, Lyon, France [Colloq. Int. C.N.R.S. **255**, 51 (1976)].
[11]L. D. Merkle, I. L. Spain, and R. C. Powell, J. Phys. C **14**, 2027 (1981).
[12]Q. Williams and R. Jeanloz, Phys. Rev. B **31**, 7449 (1985).
[13]E. S. Gaffney and T. J. Ahrens, J. Geophys. Res. **78**, 5942 (1973).
[14]T. Goto, T. J. Ahrens, and G. R. Rossman, Phys. Chem. Mineral. **4**, 253 (1979).
[15]R. W. G. Wyckoff, *Crystal Structures* (Interscience, New York, 1948), Vol. 2.
[16]D. S. McClure, J. Chem. Phys. **36**, 2757 (1962).
[17]S. Sugano, Y. Tanabe, and H. Kamimura, *Multiplets of Transition-Metal Ions in Crystals* (Academic, New York, 1970).
[18]S. Sugano and Y. Tanabe, J. Phys. Soc. Jpn. **13**, 880 (1958).
[19]R. C. Powell and B. DiBartolo, Phys. Status Solidi A **10**, 315 (1972).
[20]H. K. Mao and P. M. Bell, Carnegie Inst. Washington Year Book. **77**, 904 (1978).
[21]W. C. Moss and K. A. Goettel, Appl. Phys. Lett. **50**, 25 (1987).

[22]W. C. Moss and K. A. Goettel, J. Appl. Phys. **61**, 4951 (1987).
[23]I. F. Silvera and R. J. Wijngaarden, Rev. Sci. Instrum. **56**, 121 (1985).
[24]J. H. Eggert, K. A. Goettel, and I. F. Silvera, Appl. Phys. Lett. **53**, 2489 (1988).
[25]R. C. Powell, B. DiBartolo, B. Birang, and C. S. Naiman, J. Appl. Phys. **37**, 4973 (1966).
[26]A. Misu, J. Phys. Soc. Jpn. **19**, 2260 (1964).
[27]T. H. Maiman, R. H. Hoskins, I. J. D'Haenens, C. K. Asawa, and V. Evtuhov, Phys. Rev. **123**, 1151 (1961).
[28]R. G. Munro, J. Chem. Phys. **67**, 3146 (1977).
[29]A. P. Jephcoat, R. J. Hemley, and H. K. Mao, Physica B+C **150B**, 115 (1988).
[30]R. M. Mcfarlane, J. Chem. Phys. **39**, 3118 (1963).
[31]R. E. Cohen, Geophys. Res. Lett. **14**, 37 (1987).
[32]D. P. Ma, J. R. Chen, Z. Q. Wang, and Z. G. Zhang, Phys. Lett. A **126**, 377 (1988).
[33]S. Ohnishi and S. Sugano, Jpn. J. Appl. Phys. **21**, L309 (1982).
[34]C. W. Struck and W. H. Fonger, J. Lumin. **10**, 1 (1975).
[35]C. C. Klick and J. H. Schulman, in *Solid State Physics,* edited by F. Seitz, D. Turnbull, and H. Ehrenreich (Academic, New York, 1957), Vol. 5, p. 97.
[36]W. H. Fonger and C. W. Struck, Phys. Rev. B **11**, 3251 (1975).
[37]G. H. Watson, Jr., W. B. Daniels, and C. S. Wang, J. Appl. Phys. **52**, 956 (1981).
[38]Y. Tanabe, Suppl. Prog. Theor. Phys. **14**, 17 (1960).
[39]A. L. Schawlow, in *Advances in Quantum Electronics,* edited by J. R. Singer (Columbia University Press, New York, 1961), p. 50.
[40]E. Feher and M. D. Sturge, Phys. Rev. **172**, 244 (1968).
[41]D. M. Adams, R. Appleby, and S. K. Sharma, J. Phys. E **9**, 1140 (1976).
[42]R. C. Powell, B. DiBartolo, B. Birang, and C. S. Naiman, Phys. Rev. **155**, 296 (1967).
[43]J. M. Besson and J. P. Pinceaux, Rev. Sci. Instrum. **50**, 541 (1979).
[44]R. G. Munro, G. J. Piermarini, S. Block, and W. B. Holzapfel, J. Appl. Phys. **57**, 165 (1985).
[45]H. E. Lorenzana, H. Boppart, and I. F. Silvera, Rev. Sci. Instrum. **59**, 2583 (1988).
[46]H. K. Mao, P. M. Bell, J. W. Shaner, and D. J. Steinberg, J. Appl. Phys. **49**, 3276 (1978).
[47]D. R. Wilburn and W. A. Bassett, Am. Mineral. **63**, 591 (1978).
[48]Y. K. Vohra, S. J. Duclos, K. E. Brister, and A. C. Ruoff, Phys. Rev. Lett. **61**, 574 (1988).
[49]Y. K. Vohra, C. A. Vanderborgh, S. Desgreniers, and A. L. Ruoff, in Program of the 1989 March Meeting of the American Physical Society, St. Louis, 1989 [Bull. Am. Phys. Soc. **34**, 507 (1989)].